ELSEVIER

NeuroImage

www.elsevier.com/locate/ynimg
NeuroImage 22 (2004) 1492–1502

Semiautomatic brain region extraction: a method of parcellating brain regions from structural magnetic resonance images

L.A. Dade,[a,b,c] F.Q. Gao,[b] N. Kovacevic,[b] P. Roy,[b] C. Rockel,[b] C.M. O'Toole,[a,b] N.J. Lobaugh,[b,c] A. Feinstein,[b,c] B. Levine,[a,b,c] and S.E. Black[a,b,c,*]

[a] *Rotman Research Institute, Baycrest Centre for Geriatric Care, Canada*
[b] *Sunnybrook and Women's College Health Science Centre, Canada*
[c] *University of Toronto, Toronto Ontario, Canada*

Received 16 October 2003; revised 3 March 2004; accepted 8 March 2004

Structural MR imaging has become essential to the evaluation of regional brain changes in both healthy aging and disease-related processes. Several methods have been developed to measure structure size and regional brain volumes, but many of these methods involve substantial manual tracing and/or landmark identification. We present a new technique, semiautomatic brain region extraction (SABRE), for the rapid and reliable parcellation of cortical and subcortical brain regions. We combine the SABRE parcellation with tissue compartment segmentation [NeuroImage 17 (2002) 1087] to produce measures of gray matter (GM), white matter (WM), ventricular CSF, and sulcal CSF for 26 brain regions. Because SABRE restricts user input to a few easily identified landmarks, inter-rater reliability is high for all volumes, with all coefficients between 0.91 and 0.99. To assess construct validity, we contrasted SABRE-derived volumetric data from healthy young and older adults. Results from the SABRE parcellation and tissue segmentation showed significant differences in multiple brain regions in keeping with regional atrophy described in the literature by researchers using lengthy manual tracing methods. Our findings show that SABRE is a reliable semiautomatic method for assessing regional tissue volumes that provides significant timesavings over purely manual methods, yet maintains information about individual cortical landmarks.

Keywords: SABRE; Brain; MRI

Introduction

Advances in imaging technology have allowed for greater precision in the assessment of volumetric changes in brain tissue in vivo. Analysis of the frequency, rate, and region of tissue volume change has given rise to increased understanding and more specific hypotheses about both healthy and disease-driven processes of cerebral change. For example, regional MRI volumetric studies have revealed atrophy in the hippocampal (Jack et al., 1992; Kesslak et al., 1991; Kohler et al., 1998), parahippocampal (Kesslak et al., 1991; Kohler et al., 1998), and entorhinal (Juottonen et al., 1998) cortices in patients with Alzheimer's Disease. Similar approaches have been taken in the investigation of epilepsy (Cendes et al., 1993), frontotemporal dementia (Chan et al., 2001b; Frisoni et al., 1999; Rosen et al., 2002), schizophrenia (Barta et al., 1990; Crespo-Facorro et al., 2000), as well as normal aging (Bigler et al., 1997; Jack et al., 1992; Salat et al., 2002; Tisserand et al., 2000). Findings such as these have raised the possibility of using volumetric measures to assist in diagnosis.

Several different methods have been used to assess structure size and volume by measuring MR images. Regional volumetric measurements require careful slice-by-slice tracing of well-defined structures or specific cortical areas. Due to the labor-intensive requirements of the planimetric method, studies using this approach are typically limited to the analysis of a small number of structures. Even more simplified methods of examining structural size, such as linear measures (e.g., structural length of the hippocampus along the *y* axis, Dade et al., 2002, or medial temporal lobe width, Gao et al., 2003, 2004), can require substantial time for training. Linear measures allow for the measurement of more regions, but the time required for the user to find and evaluate the appropriate structural endpoints is significant. For example, demarcation of appropriate landmarks for linear measures of temporal lobe structures can take up to 3 h (Crane, 1999; J. Crane Personal communication, 2002). Despite the time costs of manual methods, they are often necessary to account for individual variability in the shape and course of anatomical structures.

Measurement of cortical regions of interest is particularly difficult as cerebral sulci are variable in their presence and location (Caviness et al., 1996; Ono et al., 1990; Rademacher et al., 1993). Nevertheless, several groups have developed methodologies for manual tracing and parcellation of cortical regions (Allen et al., 2002; Caviness et al., 1996; Kim et al., 2000; Rademacher et al., 1992; Tzourio-Mazoyer et al., 2002). These approaches involve identification and manual tracing of numerous specific landmark locations and have ultimately provided effective strategies for determining cortical volumes. However, localizing and tracing all

* Corresponding author. Division of Neurology, Sunnybrook and Women's Health Sciences Centre, 2075 Bayview Avenue, A421, Toronto, Ontario, Canada M4N 3M5. Fax: +1-416-480-4552.
E-mail address: blevine@rotman-baycrest.on.ca (B. Levine).
Available online on ScienceDirect (www.sciencedirect.com.)

1053-8119/$ - see front matter © 2004 Elsevier Inc. All rights reserved.
doi:10.1016/j.neuroimage.2004.03.023

the required landmarks can take several hours, even if one was evaluating only frontal cortical regions. It then takes many more hours to complete the necessary tracing to obtain volumes for regions of the entire brain. In addition, there are often difficulties in determining structural start and end points, with costs to reproducibility (Kim et al., 2000). This is particularly relevant in the measurement of neocortical regions (Caviness et al., 1996; Ono et al., 1990; Rademacher et al., 1993).

One interesting new development is a recently described automated program (Fischl et al., 2002) that uses information from MRI image intensities and spatial information about brain structures to allow automated labeling of subcortical regions. By using these two sources of information, volumes of several subcortical structures are obtained. This type of methodology alleviates operator landmark localization and errors that occur due to hand tracing. However, this method has not yet been extended to more complex neocortical divisions.

Other researchers have taken the approach of using simplified manual tracing (Bokde et al., 2002), automated evaluation of the whole brain (Chan et al., 2001a; Fox et al., 1999), or restricting analysis to total intracranial volumes (Eritaia et al., 2000). Such methods provide rapid and reliable measures of gross atrophy for between- or within-subject comparisons. However, if atrophy is present, the whole brain approach must be integrated with a method of regional parcellation to determine the specific location of the atrophy (e.g., Chan et al., 2001a), which then raises the previously stated difficulties in manual measurement.

An alternative method of identifying regional brain tissue differences between groups is voxel-based morphometry (VBM). This method typically involves spatial normalization of brain images to a template along with tissue segmentation, and then smoothing of the image to obtain a more normal distribution of the image data (Ashburner and Friston, 2000; Good et al., 2001; Watkins et al., 2001). Statistical between-group tissue comparisons are then made voxel by voxel to determine differences in tissue composition at each voxel. Advantages to this approach include its complete automation and extremely high reliability, lending itself well to analysis of large subject groups. However, the possibility has been raised that the sensitivity of VBM may not be consistent over all brain areas, as detection decreases for regions with greater anatomical variability (Quarantelli et al., 2002; Tisserand et al., 2002). In addition, VBM does not provide truly quantitative measures of tissue differences but rather provides a more qualitative analysis of regional differences. It is also not currently applicable to individual subject analyses, which limits its clinical application.

In this paper, we describe a new method, semiautomatic brain region extraction (SABRE), for parcellating cortical and subcortical regions. This approach is a meld of manual and automatic approaches and is based on user defined landmarks and regions of interest defined by the Talairach grid (Talairach and Tournoux, 1988). There are marked interindividual differences in cerebral anatomy (Ono et al., 1990). For example, Steinmetz et al. (1989) found in normal individuals using the Talairach grid that the central sulcus varied up to 2 cm in its anterior–posterior location. Accounting for these differences may be important in the study of patient populations where anatomical variability is increased, as well as in healthy subjects. SABRE combines manual tracing of a few important anatomical landmarks (providing anatomical specificity), with automated Talairach grid divisions. Regions of interest defined by Talairach grid divisions have been shown by others to have a high correspondence with manual regional tracings (Andreasen et al., 1994; Tisserand et al., 2002).

The SABRE program is used in conjunction with tissue compartment segmentation software (Kovacevic et al., 2002) to provide rapid and reliable regional volumes of gray matter (GM), white matter (WM), and cerebrospinal fluid (CSF). Following manual identification of 15 easily located landmarks, 26 brain regions (13 left, 13 right) are automatically parcellated. The entire process can be completed in less than 1 h, providing significant timesavings over manual tracing methods. We present two analyses addressing the reliability and construct validity of SABRE. Interrater reliability of the approach was assessed by two raters who independently measured images in a sample of healthy young and older adults. Construct validity was assessed by comparing and contrasting regional tissue volumes in healthy young and older adults to determine if SABRE is effective in detecting regional atrophy as described previously in the aging literature.

Methods

Participants

The scans of 10 young (mean age = 28.4, range: 22–43) and 11 older healthy adults (mean age = 78.3, range: 56–91) were used for assessing the reproducibility of SABRE-defined regional tissue compartment volumes. To evaluate SABRE's construct validity, the same 10 scans of the healthy young subjects were compared to a slightly younger sample of older adults (mean age = 66.8, range: 56–78). None of the participants had a history of neurological disease, and all older adults were living independently in the community. This study was approved by the Sunnybrook and Women's Research Ethics Board. All participants gave informed consent.

MR protocols

MR images were acquired on a 1.5 T Signa scanner (GE Medical Systems). Three image sets were required to complete the protocol: T1-weighted (axial 3D SPGR with a 5 ms TE, 35 ms TR, 1 NEX, 35° flip angle, 22 × 16.5 cm FOV, 0.859 × 0.859 mm in-plane resolution, and 1.2- to 1.4-mm-slice thickness), proton-density (PD), and T2-weighted (interleaved axial spin echo with TEs of 30 and 80 ms, 3 s TR, 0.5 NEX, 22 × 22 cm FOV, 0.859 × 0.859 mm in-plane resolution, and 3-mm-slice thickness).

Image analysis

Manual AC–PC alignment and SABRE landmark identification and tracing (described below) were completed using ANALYZE software (Biomedical Imaging Resource, Mayo foundation, Rochester, MN, USA). MR image coregistration and AC–PC transformations were completed using the Automatic Image Registration package v3.07 (Woods et al., 1998).

Initial processing of the MR images involved removing the skull and nonbrain tissues using the PD-T2-weighted images to generate a brain mask encompassing the entire intracranial cavity, excluding infratentorial cranium. As the cerebellum is not part of the Talairach coordinate system, it was also removed at this time. The final brain mask was then applied to the T1 image (Kovacevic et al., 2002). The binary mask was transformed using nearest

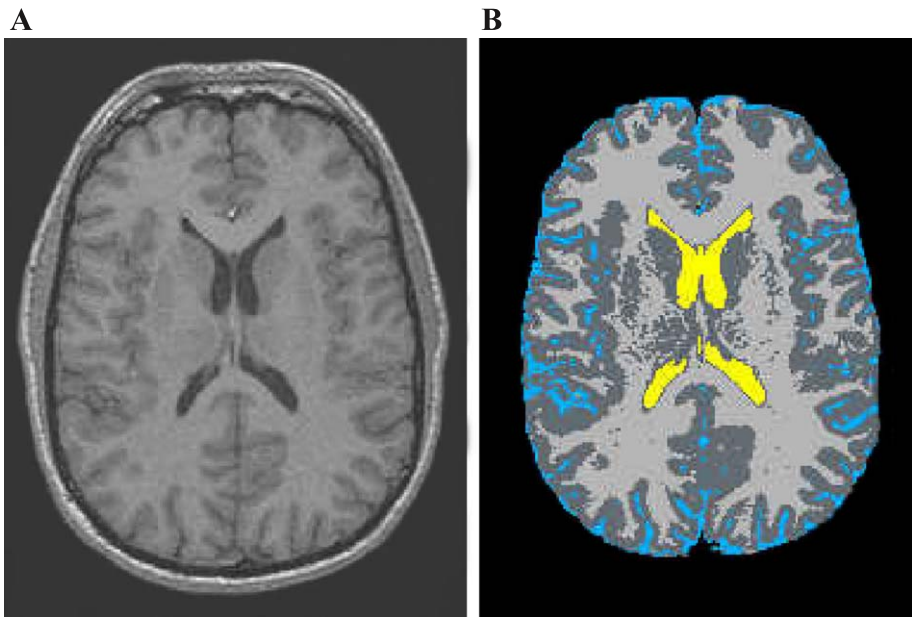

Fig. 1. (A) Original T1 image, (B) segmented image showing color-coded gray matter (dark gray), white matter (light gray), and ventricular (yellow) and subdural and sulcal CSF (blue) compartments.

neighbor interpolation. The T1 image was manually aligned along the plane passing through the anterior and posterior commissures (AC–PC), and the masked T1 image was rotated (sinc interpolation) into an isotropic AC–PC volume. The AC–PC T1 image was segmented (Kovacevic et al., 2002), and ventricular CSF voxels were identified and assigned as vCSF, with remaining CSF identified as subdural and sulcal CSF (ssCSF) (Fig. 1). A 3D "eroded" version of the acquired T1 image, with the skull and subdural CSF removed, was created for the SABRE landmarking procedure. This preprocessing step takes approximately 20 min. The SABRE mask was then created and applied to the edited segmented image to derive tissue volumes for 26 regions.

Semiautomatic brain region extraction

Our selection of the 26 regions (13 per hemisphere) was governed by major anatomical divisions (e.g., separation of cortical lobes), distinctions of theoretical interest in patients with brain disease (e.g., separation of lateral from medial frontal regions), and practical considerations, namely the optimization of reliability and efficiency. The standard Talairach atlas (Talairach and Tournoux, 1988) was used as a guide to make initial estimates of borders between regions. To minimize regional misclassification of tissue due to individual variations in brain anatomy, criteria for boundaries of problematic regions (i.e., medial temporal and inferior frontal/anterior temporal) were modified until there was consensus across the 10 brains that the divisions were appropriate (completed by authors FQG and LAD). An experienced neurologist (SEB) provided final affirmation of the boundary definitions.

Three steps are required to obtain the SABRE regional divisions and tissue volumes: (1) 15 landmarks are identified on the eroded AC–PC aligned T1 volume, (2) an individual Talairach grid is created automatically, and (3) the SABRE algorithm automatically delineates 26 brain regions. These three steps can be completed in approximately 20 min. The following sections provide an overview of these steps; additional technical information is presented in the Appendices.

Manual landmark identification

Fifteen landmarks are used to provide boundaries for the anatomical regions and to provide coordinates for the creation of an individualized Talairach grid for each brain image (see Fig. 2). Coordinates for the following seven landmarks are obtained from the AC–PC aligned T1 image: (1) the z (superior–inferior) coordinate defining the top of the anterior and posterior commissures (AC–PC); (2 and 3) the y (anterior–posterior) coordinates indicating the coronal planes anterior to the anterior commissure (ac); and anterior to the posterior commissure (pc); (4) the posterior midpoint coronal slice, which is the halfway point between the pc and the posterior edge of the brain; (5 and 6) the most inferior points of the left and right pre-occipital notch (Lpron, Rpron); and (7) the midline slice dividing the hemispheres (m).

The remaining eight landmarks are traced on 3D-rendered eroded AC–PC T1 images, four on each hemisphere: central sulcus (C), superior midline point of the central sulcus (mC), sylvian fissure (SF), and the parieto-occipital sulcus (poc). Rules for tracing were derived from Ono et al. (1990) (see Appendix A). These tracings are used to define the major boundaries between the four brain lobes. All sulcal tracings are automatically projected through the hemisphere from lateral to medial aspects to complete the regional boundaries, and projected out to the edge of the image volume so that ssCSF is included in the final tissue volumes.

Automatic proportional Talairach grid

Transformation or warping of brain images into a standardized Talairach space (Talairach and Tournoux, 1988) is a common procedure used to correct for individual differences in brain shape and size. However, when these image transformations are made

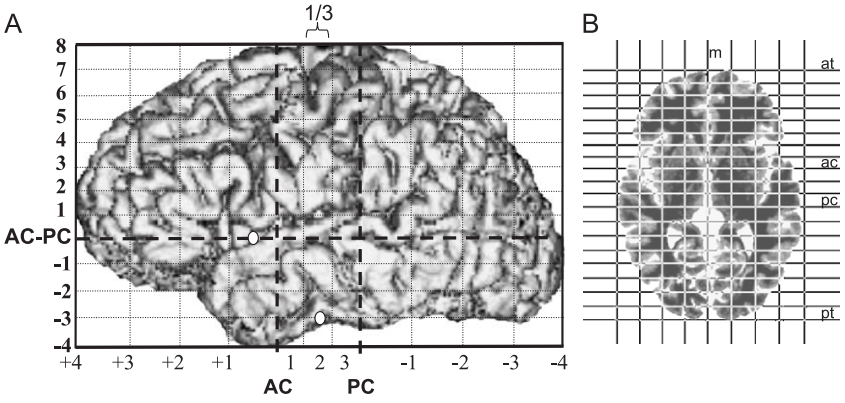

Fig. 2. (A) Example of an individualized Talairach grid on an eroded brain image. AC = anterior commissure, PC = posterior commissure. White circles indicate points used to designate the anterior and posterior temporal lobe division. (B) Axial view with Talairach grid. m = midline, at = anterior, pt = posterior.

important subtleties of structural information about an individual's brain can be lost. Therefore, to maintain the individual shape variability and correct for differences in intracranial capacity, the SABRE program creates a proportional Talairach grid (Talairach and Tournoux, 1988) for each individual's AC–PC aligned image (Fig. 2).

The extreme top, bottom, left, and right edges of the eroded image are determined automatically and define the edges of the Talairach bounding box. In the anterior to posterior direction, four equal divisions are created anterior to the AC and posterior to the PC. The region between the AC and PC is divided into three equal sections. From superior to inferior, the brain is divided into eight equal divisions above the AC–PC, and into four equal divisions below the AC–PC. Each of the left and right hemispheres is divided into four equal sagittal regions (see Fig. 2b). This creates equivalent proportional divisions of each subject's cortical tissue.

Regional definition

The landmark coordinates are combined with the proportional Talairach grid coordinates to divide the each individual's brain into 26 equivalent proportional cortical regions: 13 in the left hemisphere and 13 in the right. The divisions shown in Fig. 3 include lateral and medial superior frontal (LSF, MSF), lateral and medial middle frontal (LMF, MMF), lateral and medial inferior frontal (LIF, MIF), superior parietal (SP), inferior parietal (IP), occipital (O), anterior temporal (AT), medial temporal (MT), posterior temporal (PT), and basal ganglia and thalamus (BGT).

Frontal lobe. The frontal lobe is divided into six regions: inferior, middle, and superior, each separated into medial and lateral divisions (Fig. 3A; Appendix A.2.1). The medial inferior frontal region would be similar to the orbitofrontal region as described by Salat et al. (2001) and Salat et al. (2002). The lateral inferior frontal region is separated from the anterior temporal region by the sylvian fissure trace and a series of angled lines that vary incrementally at specified levels below the AC–PC line (Fig. 3B, arrows; Appendix A.2.1).

Parietal lobe. The parietal lobe is divided into superior and inferior regions (Fig. 3A; Appendix A.2.2). The division between superior and inferior regions occurs at the same axial slice as for the superior and middle frontal regions.

Temporal lobe. The temporal lobe is divided into three regions: anterior, posterior, and medial (Fig. 3A; Appendix A.2.3). The extent of the medial temporal lobe region was based initially on Talairach atlas coordinates and was refined to largely encompass hippocampus, amygdala, parahippocampal, and entorhinal cortices in our test brains (Appendix A.2.3).

Occipital lobe. The parietal–occipital sulcus forms a natural division between the parietal and occipital lobes. The occipital and temporal lobes are separated by a straight line (OT) calculated to drop vertically from the intersection of the parieto-occipital sulcus and the TP line (Appendix A.2.4).

Basal ganglia and thalamus. For the present implementation, the basal ganglia and thalamus are combined into a single region (Fig. 3B). An automated linear algorithm based on the Talairach atlas (Talairach and Tournoux, 1988) is used to demarcate the area of the basal ganglia and thalamus (see Appendix A.2.5 and Fig. 3B).

Segmented tissue volumes

Regional volumes of GM, WM, vCSF, and ssCSF were obtained automatically by applying the SABRE mask to the segmented AC–PC T1 image (Fig. 1). Across subjects, the regional volumes represent equivalent proportions of total brain volume, thus providing a correction for individual differences in head size. Volumes for each tissue compartment within regions are expressed as percentages of the regional volume. Regions of atrophy would be indicated by a significantly greater percent of sulcal or ventricular CSF in that region in one group compared to another. Not all brain regions have ssCSF or vCSF measures (e.g., BGT).

Inter-rater-reliability analysis

Two trained and experienced operators (FQG and PR) identified the SABRE coordinates on a series of 21 scans, which had been previously AC–PC aligned and segmented. Inter-rater reliability on the 26 regional tissue volumes was assessed using the intraclass correlation coefficient (ICC) using a two-way random effects model (Shrout and Fleiss, 1979). Coefficients were calculated for total regional volumes (across all tissue compartments), as well as for the separate regional tissue compartments.

Results

Total volume ICCs ranged between 0.97 and 0.999 for the left hemisphere and 0.91–0.998 for the right. The confidence intervals averaged ±0.03, and the mean difference between left and

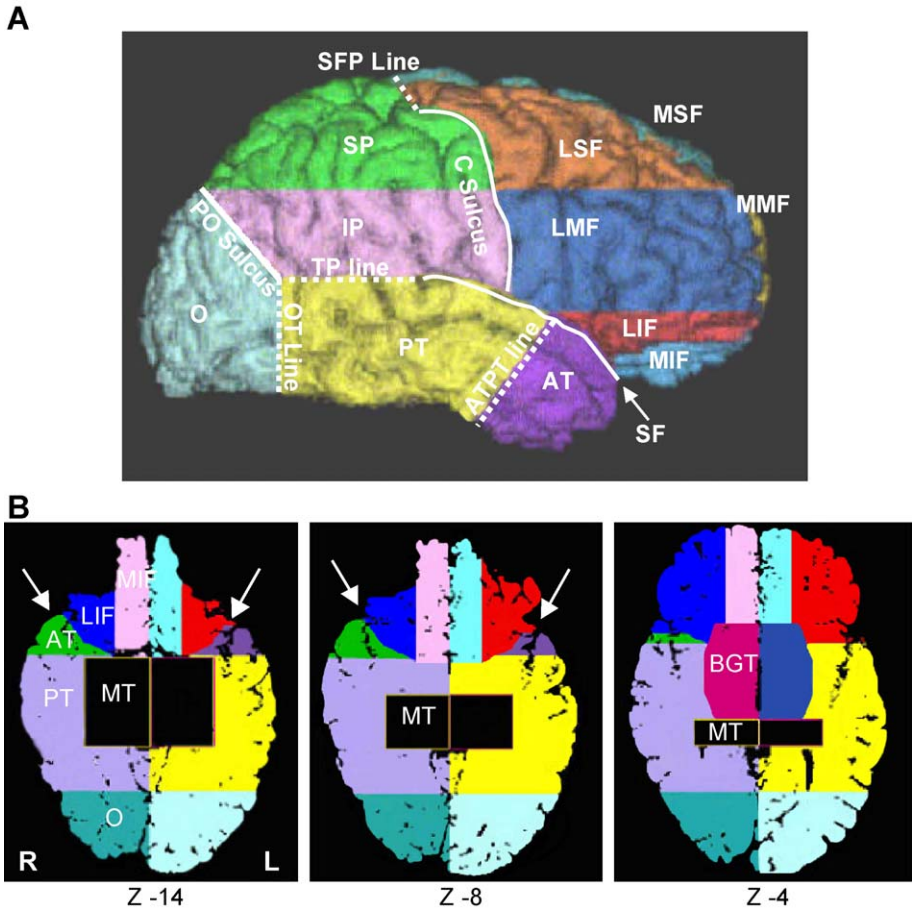

Fig. 3. SABRE regional cortical divisions in lateral and horizontal views. Three axial views at horizontal divisions approximately equal to Talairach $z = 14$, $z = -8$, $z = -4$. Abbreviations: LSF = lateral superior frontal, MSF = medial superior frontal, LMF = lateral middle frontal, MMF = medial middle frontal, LIF = lateral ventral frontal, MIF = medial ventral frontal, SP = superior parietal, IP = inferior parietal, O = occipital, AT = anterior temporal, MT = medial temporal, PT = posterior temporal, BGT = basal ganglia and thalamus, X = sagittal coordinate in Talairach space, C Sulcus = central sulcus, PO sulcus = parieto-occipital sulcus, SF = sylvian fissure, SFP line = superior–frontal–parietal dividing line, ATPT line = division between anterior and poster temporal lobe, OT line = occipital–temporal dividing line.

right ICCs for the different regions was 0.005. As there were no meaningful differences between ICC's for homologous left and right regions, regional data were collapsed across the hemispheres, yielding 13 regions. Not surprisingly, intraclass correlations remained high for all regions (0.95–0.99), with measurements for only five regions falling below 0.98 (anterior temporal, posterior temporal, basal ganglia and thalamus, superior parietal, and inferior parietal). The majority of areas with slightly lower ICCs (0.95–0.97) were defined in part by sulcal tracings, which may have added a small amount of variability. Intraclass correlations for individual tissue compartments (GM, WM, ssCSF, and vCSF) in each region were also high, ranging between 0.97 and 0.99. These data confirm SABRE's high inter-rater reliability.

Construct validity analysis

To assess SABRE's construct validity, regional volumes were compared between healthy younger and older adults and examined in the context of published age-related global (Greenwood, 2000) and regional volume differences (Raz, 2000; Raz et al., 1997; Resnick et al., 2003). Although aging is associated with generalized brain volume loss (Greenwood, 2000), several studies have shown that this loss is greatest over the frontal lobes, particularly in frontal gray matter (Raz, 2000; Raz et al., 1997).

A single trained and experienced operator (FQG) identified the SABRE landmarks on 20 participants' scans. As there were no differences across right and left hemispheres, data were averaged across hemispheres for the sake of simplicity. Tissue compartment volumes are expressed as a percent of the total volume for each region. Regions of atrophy would be indicated by a significantly greater percentage of sulcal or ventricular CSF (and corresponding loss of GM and/or WM) in that region in one group compared to another.

The effects of age on tissue volumes within the SABRE-defined regions were assessed with mixed-design ANOVAs. Only five of the regions (MMF, IP, MT, PT, O) contained all four tissue types, and ventricular and sulcal/subdural CSF types were not equally represented across these areas. To avoid listwise deletion of regions that did not contain ssCSF or vCSF tissue types, three separate analyses were conducted for parenchymal and CSF compartments. The first Group by Region by Tissue type ANOVA was restricted to gray and white matter tissue compartments and included all 13

regions. The second analysis focused on vCSF and ssCSF differences and included the five regions containing both vCSF and ssCSF compartments: medial middle frontal, inferior parietal, medial temporal lobe, posterior temporal lobe, and occipital lobe. A final ANOVA examined the Group by Region effect for the remaining ssCSF volumes: superior and inferior frontal (lateral and medial divisions), lateral middle frontal, superior parietal, and anterior temporal regions. Significant interactions were decomposed with simple effect analyses using a pooled error term.

Results

Percentages of GM and WM for each region are presented in Fig. 4. For parenchymal compartments (GM and WM), a significant main effect for group, $F_{1,18} = 31.4$, $P < 0.001$, confirmed expected age-related generalized atrophy. This atrophy, however, was not consistent across regions and tissue compartments, as indicated by a three-way interaction, $F_{12,216} = 2.09$, $P < 0.019$. Regional Group by Tissue type analyses indicated significantly greater tissue loss in gray matter than white matter for the older adults in two regions: lateral superior frontal, $F_{1,234} = 5.03$, $P < 0.03$, and lateral inferior frontal cortices, $F_{1,234} = 4.3$, $P < 0.04$. A Group by Region analysis revealed a significant overall volume loss in the elderly in all regions, except the basal ganglia/thalamus division.

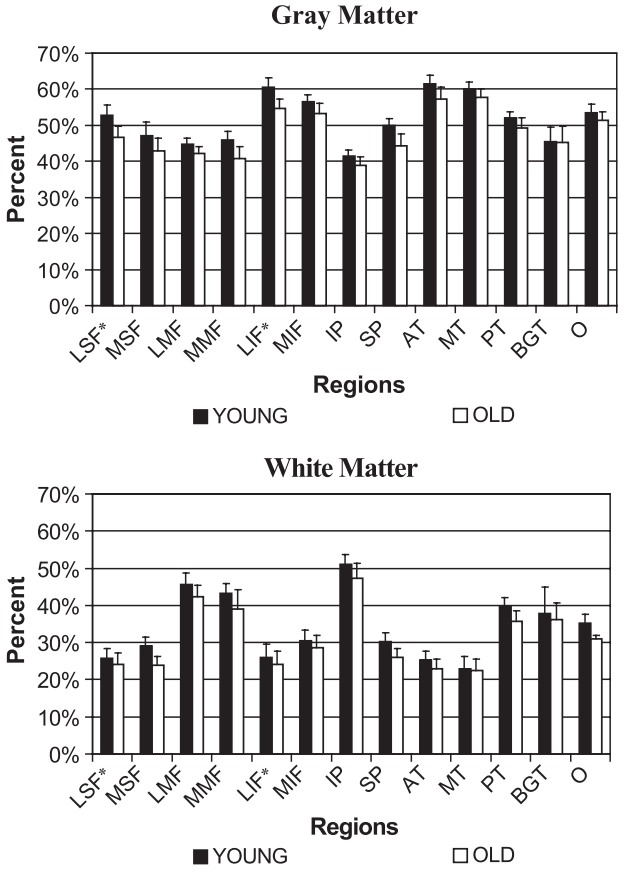

Fig. 4. Regional gray and white matter volumes in young and old groups. Gray and white volumes are presented as a percentage of total regional volume. Abbreviations as in Fig. 3. There was a significant overall volume loss in the old as compared to the young in all regions, with the exception of the BGT division. *In comparison to other regions, older adults showed significantly greater loss of gray matter than white matter in LSF and LIF regions ($P < 0.04$).

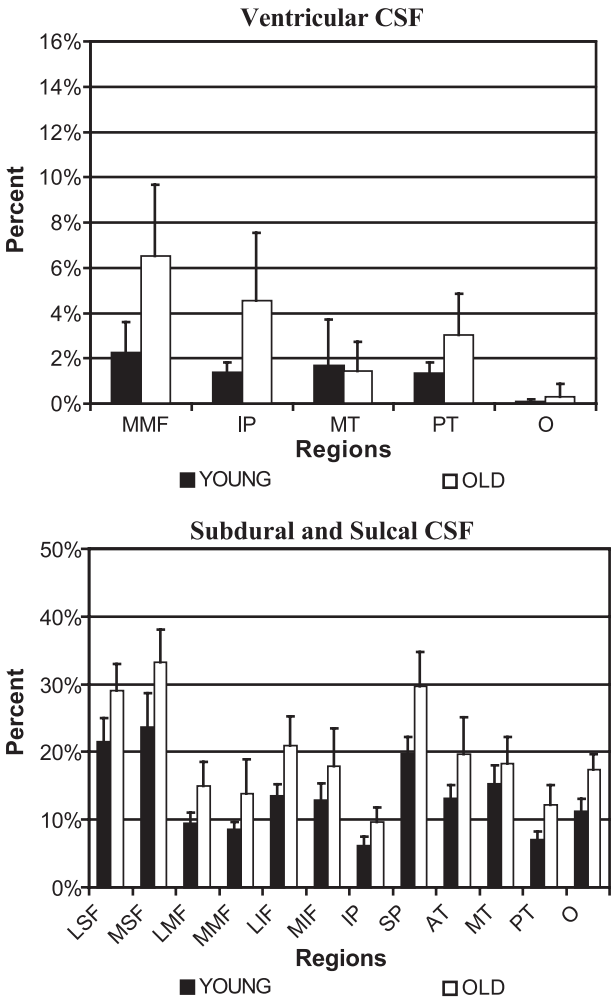

Fig. 5. Regional ventricular CSF and subdural/sulcal CSF volumes in young and old groups. Abbreviations as in Fig. 3. In the five regions that contained both vCSF and ssCSF (MMF, IP, MT, PT, O), a significant Age by Region by CSF-type effect showed that older adults had significantly greater ssCSF in MT, PT, and O regions.

The analysis of regions containing both vCSF and ssCSF (MMF, IP, MT, PT, O) (Fig. 5) revealed the expected significant group effect of larger CSF volumes in the older group ($F_{1,18} = 26.96$, $P < 0.001$). Once again, a significant Region by Tissue Type by Group interaction ($F_{4,72} = 4.9$, $P < 0.001$) indicated that this effect was not equivalent across regions. Post hoc analyses showed significant interactions in the occipital lobe ($F_{1,90} = 2.4$, $P < 0.01$), and medial ($F_{1,90} = 7.2$, $P < 0.01$) and posterior ($F_{1,90} = 8.1$, $P < 0.01$) temporal lobe regions. In these regions, there was a significantly greater volume of ssCSF in older adults as compared to younger adults, and this volume difference was larger than the group difference in ventricular vCSF volumes (see Fig. 5).

The final analysis of CSF differences examined the five regions containing only ssCSF areas. Older individuals showed the expected effect of increased CSF volume ($F_{1,18} = 46.2$, $P < 0.001$), but there was no Group by Region interaction. These results reflect the main effect of age as shown in the gray and white matter analyses.

Discussion

Regional tissue compartment segmentation results demonstrate that SABRE can illuminate specific patterns of atrophy between groups. Although the sample sizes are small, the effects replicate prior findings in the literature of gray and white matter changes with age (see Raz, 2000, for review), supporting the validity of this approach.

Older adults had lower gray and white matter volumes than younger adults over the majority of brain regions (Fig. 4). Moreover, SABRE revealed differential tissue loss in specific frontal lobe areas. Frontal lobes of older subjects showed significantly greater loss of gray matter than white matter in lateral superior and inferior frontal regions. These findings reflect both the general findings in the literature of gray and white matter tissue loss in frontal regions (Raz et al., 1997; Resnick et al., 2000, 2003; Salat et al., 2001; Tisserand et al., 2002), and a more specific finding of greater gray than white matter loss (Raz, 2000; Raz et al., 1997). Greater gray matter loss was not noted in the lateral middle frontal region, possibly because a few subjects had extension of ventricular CSF spaces into the lateral middle frontal region, resulting in a lower white matter volume. This would result in a less substantial difference between gray and white matter volumes, and thereby diminish the magnitude of the gray–white disparity in this region. This is a finding that could be pursued more systematically in a larger sample of subjects.

Few volumetric methodologies allow for comparisons of ventricular and extracortical subdural and sulcal CSF volumes. Some approaches do not divide the fluid spaces (e.g., Guttmann et al., 1998), while others measure only ventricular CSF (e.g., Allen et al., 2002). Other quantitative brain image analysis approaches do not give measures of sulcal CSF volumes (Goldszal et al., 1998; Resnick et al., 2000) as the method for extraction of extracranial tissue results in inconsistent removal of areas of sulcal CSF. Manual tracing methods also generally focus on gray and white matter tissue regions of the neocortex, and rarely include a measure of sulcal CSF. The combination of the SABRE approach with segmentation methodology that defines subdural and sulcal CSF (Kovacevic et al., 2002) has allowed us to examine both types of CSF volumes in the regional divisions. The segmentation methodology (Fig. 1) permits examination of the regional specificity of age effects across cerebral spinal fluid compartments (Fig. 5) and allows more detailed analyses of the effects of atrophy. Additionally, the finding of greater increases in sulcal and subdural CSF compared to ventricular CSF in temporal lobe regions is in keeping with Pfefferbaum et al. (1994) who found greater increases in cortical CSF volume relative to ventricular CSF in aging. Our present results are also interesting as they contrast with the increase in ventricular CSF that occurs following atrophy in chronic traumatic brain injury (Bigler et al., 1992; Levine et al., 2002), suggesting that different causes of brain atrophy do not lead to the same pattern of fluid volume distribution.

General discussion

Regional measures of brain volume from structural neuroimages are promising for both research and clinical applications, yet few cost-effective techniques have been systematically validated. This study addressed the reliability and validity of SABRE, an integrated, time-efficient approach to the parcellation of brain regions.

SABRE requires approximately 20 min for landmark identification and is easily integrated with any segmented image to generate regional volumes of gray matter, white matter, CSF compartments. The initial step in evaluating this approach was to examine the consistency of regional volumes created by the SABRE system as defined by two trained and independent raters. The very high resultant ICCs for the 13 hemispheric regions supported the reliability of this approach. The construct validity of SABRE was supported by the demonstration of predicted regional volume loss in young and old healthy adults.

SABRE, although similar in many ways to other parcellation techniques, has certain features that will increase its utility. For example, Bokde et al. (2002) have developed a similar regional landmark based protocol, although manual tissue segmentation is required. An important disadvantage relative to our approach is that large regions such as the frontal and temporal lobes are not subdivided; additional parcellation approaches would be necessary to interpret local tissue differences. Other researchers have implemented techniques that parcel the brain into smaller regions. For instance, Kim et al. (2000) have developed an approach to examine 16 regions within the temporal lobe. This method uses manual parcellation on a 3D, slice-by-slice, image-analysis approach. Although intraclass correlations were generally high, they were not uniformly so (range: 0.62–0.99) in spite of the significant amount of training and the time-intensive tracing involved.

Andreasen et al. (1996) and Quarantelli et al. (2002) have utilized a similar method that involves automatic assignment of image voxels to frontal, parietal, occipital, and temporal lobes according to the Talairach atlas. Voxels are labeled based on the defined atlas, without taking individual sulcal boundaries into account. For the large part, these methods correlated well with manual tracing approaches and provide accurate measures of brain lobes. However, it was noted that this type of automated approach, although highly efficient, is not suitable when there are alterations in the normal anatomy (Quarantelli et al., 2002), as can occur in pathological conditions such as Alzheimer's disease or frontotemporal dementia. These methods are also less accurate in labeling tissue near sulcal landmarks, such as the central sulcus and the sylvian fissure, due to the substantial variability across individuals (Andreasen et al., 1996; Ono et al., 1990; Steinmetz et al., 1989). Hence, a fully automated method based solely on grid divisions without consideration of individual anatomical differences may not lead to accurate volume measures in certain patient populations where variability is increased. Because the approach taken with SABRE utilizes manual tracing of these landmarks, individual differences and differences in these sulci due to pathological changes can be taken into account when making regional volume measures. Thus, SABRE may prove to be a more sensitive measure for certain patient populations than fully automated atlas-based approaches.

Caviness et al. (1996) presented a detailed manual parcellation method to divide the brain into 48 units. This technique was a refined version of an earlier approach presented by Rademacher et al. (1992). It involves the identification of 42 anatomical landmarks (38 of which are located by the operator) as well as the tracing of 34 fissures. Inter-rater reliability was near perfect for a sample of young, healthy brains. Although this method is promising, it assumes a high level of knowledge and experience in the operators as well as numerous hours of training. This methodology, developed using images of 3-mm-slice thickness, was reported to take

skilled investigators hours to complete, and would double or triple in time when applied to higher resolution images.

The SABRE method provides timesavings, which is important in both the context of large group studies, and within a clinical environment. However, this technique is not without some limitations. The regional divisions were based on a combination of naturally occurring anatomical regions and parsimonious linear divisions that were employed in areas where tracing methods became laborious or less reliable. This results in regional divisions that do not strictly follow gross anatomical regions or cytoarchitectonic divisions. Therefore, this methodology will not be applicable to those researchers who are interested in exact tissue volumes of a specific gyrus or of small brain regions. Nevertheless, the SABRE program is relatively adaptable and new algorithms can be added to the program to examine regions of interest more closely. For example, we are currently examining approaches for creating reliable divisions of the cingulate gyrus.

Without an empirical test, it remains to be seen if the SABRE approach would be more accurate than a purely automated approach. One of our future goals is to answer the question of whether this more specific form of semiautomated measurement will help to elucidate differences in patient populations where anatomical variability between individuals will be large, as in dementia and traumatic brain injury. We have already demonstrated SABRE's capacity to detect frontal and anterior temporal lobe volume differences between depressed and nondepressed MS patients (Feinstein et al., 2004).

Given the current absence of reliable automatic tracing of anatomical landmarks, researchers must make decisions about the desired balance between preserving anatomical detail and the time required to attain reliable measures at this level of detail. Relative to other tracing methods, the semiautomatic SABRE approach offers a reliable, valid, and temporally economical option. This system can be easily applied in large group studies where divisions based on individual landmarks are desired without the intensive labor involved in tracing of numerous sulci. It can also be utilized as a primary step to elucidate regions of difference quickly, perhaps leading to a more detailed investigation. Another advantage of the SABRE system is that it maintains individual differences through integrating individually traced landmarks while dividing areas into equivalent proportional regions. Maintenance of these individual differences is minimized when brains are typically transformed into standardized space, resulting in a loss of the brain's topographical uniqueness. Although we have maintained some of the individual markers in our approach, we have also been able to decrease the number of individual landmarks to be identified. This should minimize differences in volume measures due to variability in investigator/operator performances, and result in more reliable and meaningful analyses of regional tissue compartments.

Acknowledgments

This work was supported by Canadian Institutes of Health Research grant 13129 to Dr. S.E. Black, grants 15001 and 36535 to Dr. A. Feinstein, and grant 37535 to Dr. B. Levine. As well as by NIH grant 42385 and an Ontario Premier's Research Excellence Award to Dr. Levine. We thank the subjects who participated in this experiment, and Joel Ramirez for his assistance with the image analysis. We also thank Malcom Binns for consultation on statistical issues.

Appendix A

A.1. Landmarks

All landmarks are located manually on the AC–PC aligned T1 image.

The AC–PC line. The z (inferior–superior) coordinate where the tops of the anterior (AC) and posterior (PC) commissures are observable.

AC and PC points. The *x* (medial–lateral) and *y* (anterior–posterior) coordinates anterior to the AC and PC obtained at the level of the AC–PC plane. These coordinates are used to create the Talairach grid and to define some regional boundaries.

Posterior midpoint. In the AC–PC plane, the *y* coordinate halfway between the PC and the posterior edge of the brain defines the coronal slice from which the pre-occipital notch (pron) is determined.

Pre-occipital notch (pron: left and right). The lowest *z* coordinates for the left and right occipital cortices on the posterior midpoint coronal slice. These landmarks are used to define the endpoints of the occipital–temporal lines (OT).

Midline (m). The *x* coordinate in the center of the cerebral aqueduct, 10 axial slices below the AC–PC plane. It defines the division between left and right hemispheres.

Central sulcus (C). The central sulcus extends obliquely between the precentral and postcentral gyri. There is commonly a bridge between the precentral and postcentral gyri that interrupts the inferior portions of the central sulcus (Ono et al., 1990). When this occurs, the two sections of the central sulcus are connected with a straight vertical line. The superior endpoint of the central sulcus is determined by either the turning point of the sulcus from the lateral surface to the superior medial surface, or by the joining point of a "Y" or "T" termination (Ono et al., 1990).

Sylvian fissure (SF). Anterior tracing of the Sylvian fissure commences just below the point of curvature of the anterior temporal lobe. The end point is determined at one of three possible anatomical markers: (1) the bifurcation of the terminal ascending segment and posterior transverse temporal sulcus (most common), (2) the bifurcation of a ramified end, or (3) at its simple end (a straight end without obvious branches, rarely seen) (Ono et al., 1990).

Medial point of the central sulcus (mC). The superior portion of the central sulcus is not visible from the lateral view. To complete this upper portion, we took a simplified approach of obtaining the mC point at seven sagittal slices lateral to the midline plane. A point is placed on the central sulcus, which is then automatically connected to the central sulcus tracing to form the superior frontal–parietal line (SPF line).

Parieto-occipital sulcus (PO). The parieto-occipital sulcus is a consistent landmark on the posterior medial surface of the brain. It is traced on the same sagittal slice as mC, inferiorly from the intersection point with the tentorium along the center of the sulcus to its most superior point. At the surface of the cortex, the line is projected out to the edge of the image volume.

A.2. Regional boundaries

Coordinates defined below are expressed relative to the Talairach reference planes as the number of grid coordinates [e.g., vPC(−2) = two *vertical* grid lines posterior to the PC; Fig. 2].

A.2.1. Frontal lobe

Posterior border. This consists of the central sulcus tracing with automated extensions at the superior and inferior ends. The central sulcus tracing is connected to the mC point creating the superior frontal–parietal (SFP) line. From the inferior point of the central sulcus, a vertical line is dropped down to AC–PC(−0.5) to complete the posterior boundary. For middle and inferior regions, the posterior border is defined by the central sulcus or the sylvian fissure, depending on which line is first encountered in the *z* plane for that particular image.

Divisions between inferior, middle, and superior frontal regions. The AC–PC plane creates the division between inferior and middle frontal (Callen et al., 2001). Superior and middle frontal regions are divided at AC–PC(+4), the midpoint between the AC–PC plane and the top of the brain.

Medial and lateral frontal regions. These divisions occur at the Talairach grid midline(±1).

Inferior frontal regions. The inferior frontal demarcation is more complex to minimize inclusion of tissue in the anterior temporal lobe. The division between inferior frontal and anterior temporal regions consists of four angled line segments extending from midline to the outer edge of the brain. The placement of these lines was confirmed on our series of test brains. The angles of these lines (arrows, Fig. 3B) vary incrementally at seven specified *z* levels between AC–PC(0) and AC–PC(−2.5).

A.2.2. Parietal lobe

Anterior and posterior borders. The central sulcus tracing and SFP line define the anterior border, and the parietal–occipital sulcus tracing defines the posterior border.

Division between superior and inferior regions. The parietal lobe is divided at the same level used for the frontal regions [AC–PC(+4)].

Inferior parietal/temporal border. The sylvian fissure forms the anterior portion of the division, which is completed by the temporal–parietal line (TP line). The TP line is parallel to the AC–PC plane and extends from the most posterior point of the sylvian fissure to the intersection of the parietal–occipital sulcus and the occipital–temporal line (OT line, below).

A.2.3. Temporal lobe

Superior and anterior borders. The superior border is defined by the sylvian fissure and the temporal–parietal line. The anterior border is the inferior frontal demarcation (above).

Division between AT and PT. The ATPT line starts at the bottom of the brain and is drawn from vAC(−1.5), AC–PC(−3) to vAC(+0.5), AC–PC(0). The line continues upward until it intersects with the sylvian fissure (Figs. 2, open dots, and 3A).

Medial border of AT and PT. Anterior and posterior to the MT, the medial border is the hemispheric midline ($x = 0$). For all other slices, the medial border is defined by the MT (M ± 2).

Medial temporal region (MT). This region begins in the inferior temporal lobe near the ATPT line and progresses up through the posterior temporal region to the level of the basal ganglia and thalamus. The MT extends sagitally from midline (M) to M(±2 sagittal grid divisions). The superior–inferior boundaries are at AC–PC to AC–PC(−4). At the most inferior level (AC–PC), the anterior–posterior extent is from vAC (+0.5) to vAC (−2). From here, the region is moved smoothly up and back through the MT, such that the anterior–posterior extent at the most superior level (AC–PC [−4]) is from vAP (−0.5) to vAP (−1).

A.2.4. Occipital lobe

The parietal–occipital sulcus, one of the manually traced landmarks (Appendix A), forms a natural division between the parietal and occipital lobes. The SABRE program automatically truncates the tracing at vPC(−2). At this point, the occipital temporal line (OT line) is drawn automatically along vPC(−2), terminating inferiorly at the parietal occipital notch (Fig. 3A).

A.2.5. Basal ganglia and thalamus (BGT)

This region consists of a series of polyhedra through the midbrain. The inferior–superior extent of this region is from AC–PC(−0.5) to AC–PC(+2). To account for the changes in shape of these structures, the regional definition is modified: (1) between AC–PC(−0.5) to AC–PC(−0.25), the maximal extents of the polygon are from vAC(+2) to vAC(−1) and M(±1.66); (2) at AC–PC(−0.25) to AC–PC(+1.5), the polygon is enlarged in the anterior–posterior direction and extends from vAC(+2) to vPC(−0.5) and M(±1.66); (3) at ACPC +1.5 to +2.0, the shape changes to a rectangle, from vAC(+2) to vPC(−0.5) and M(±1.0).

References

Allen, J.S., Damasio, H., Grabowski, T.J., 2002. Normal neuroanatomical variation in the human brain: an MRI-volumetric study. Am. J. Phys. Anthropol. 118, 341–358.

Andreasen, N.C., Flashman, L., Flaum, M., Arndt, S., Swayze, V., O'Leary, D.S., Ehrhadt, J.C., Yuh, W.T.C., 1994. Regional brain abnormalities in schizophrenia measured with magnetic resonance imaging. J. Am. Med. Assoc. 272, 1763–1769.

Andreasen, N.C., Rajarethinam, R., Cizadlo, T., Arndt, S., Swayze, V., Flashman, L., O'Leary, D.S., Ehrhadt, J.C., Yuh, W.T.C., 1996. Automatic atlas-based volume estimation of human brain regions from MR images. J. Comput. Assist. Tomogr. 20, 98–106.

Ashburner, J., Friston, K.J., 2000. Voxel-based morphometry—The methods. NeuroImage 11, 805–821.

Barta, P.E., Pearlson, G.D., Powers, R.E., Richards, S.S., Tune, L.E., 1990. Auditory hallucinations and smaller superior temporal gyral volume in schizophrenia. Am. J. Psychiatry 147, 1457–1462.

Bigler, E.D., Kurth, S.M., Blatter, D., Abildskov, T.J., 1992. Degenerative changes in traumatic brain injury: post-injury magnetic resonance identified ventricular expansion compared to pre-injury levels. Brain Res. Bull. 28, 651–653.

Bigler, E.D., Blatter, D.D., Anderson, C.V., Johnson, S.C., Gale, S.D., Hopkins, R.O., Burnett, B., 1997. Hippocampal volume in normal aging and traumatic brain injury. Am. J. Neuroradiol. 18, 11–23.

Bokde, A.L., Teipel, S.J., Zebuhr, Y., Leinsinger, G., Gootjes, L., Schwarz, R., Buerger, K., Scheltens, P., Moeller, H.J., Hampel, H., 2002. A new rapid landmark-based regional MRI segmentation method of the brain. J. Neurol. Sci. 194, 35–40.

Callen, D.J., Black, S.E., Gao, F., Caldwell, C.B., Szalai, J.P., 2001. Beyond the hippocampus: MRI volumetry confirms widespread limbic atrophy in AD. Neurology 57, 1669–1674.

Caviness Jr., V.S., Meyer, J., Makris, N., Kennedy, D.N., 1996. MRI-based topographic parcellation of human neocortex: an anatomically specified method with estimate of reliability. J. Cogn. Neurosci. 8, 566–587.

Cendes, F., Andermann, F., Gloor, P., Evans, A., Jones-Gotman, M., Watson, C., Melanson, D., Olivier, A., Peters, T., Lopes-Cendes, I., et al., 1993. MRI volumetric measurement of amygdala and hippocampus in temporal lobe epilepsy. Neurology 43, 719–725.

Chan, D., Fox, N.C., Jenkins, R., Scahill, R.I., Crum, W.R., Rossor, M.N., 2001a. Rates of global and regional cerebral atrophy in AD and frontotemporal dementia. Neurology 57, 1756–1763.

Chan, D., Fox, N.C., Scahill, R.I., Crum, W.R., Whitwell, J.L., Leschziner, G., Rossor, A.M., Stevens, J.M., Cipolotti, L., Rossor, M.N., 2001b. Patterns of temporal lobe atrophy in semantic dementia and Alzheimer's disease. Ann. Neurol. 49, 433–442.

Crane, J., 1999. Right Medial Temporal-Lobe Contribution to Object-Location Memory. Doctoral Thesis. McGill University, Montreal.

Crespo-Facorro, B., Kim, J., Andreasen, N.C., O'Leary, D.S., Magnotta, V., 2000. Regional frontal abnormalities in schizophrenia: a quantitative gray matter volume and cortical surface size study. Biol. Psychiatry 48, 110–119.

Dade, L.A., Zatorre, R.J., Jones-Gotman, M., 2002. Olfactory learning: convergent findings from lesion and brain imaging studies in humans. Brain 125, 86–101.

Eritaia, J., Wood, S.J., Stuart, G.W., Bridle, N., Dudgeon, P., Maruff, P., Velakoulis, D., Pantelis, C., 2000. An optimized method for estimating intracranial volume from magnetic resonance images. Magn. Reson. Med. 44, 973–977.

Feinstein, A., Roy, P., Lobaugh, N., Feinstein, K., O'Connor, P., Black, S.E., 2004. Structural brain abnormalities in multiple sclerosis patients with major depression. Neurology 62, 586–590.

Fischl, B., Salat, D.H., Busa, E., Albert, M., Dieterich, M., Haselgrove, C., van der Kouwe, A., Killiany, R., Kennedy, D., Klaveness, S., et al., 2002. Whole brain segmentation: automated labeling of neuroanatomical structures in the human brain. Neuron 33, 341–355.

Fox, N.C., Scahill, R.I., Crum, W.R., Rossor, M.N., 1999. Correlation between rates of brain atrophy and cognitive decline in AD. Neurology 52, 1687–1689.

Frisoni, G.B., Laakso, M.P., Beltramello, A., Geroldi, C., Bianchetti, A., Soininen, H., Trabucchi, M., 1999. Hippocampal and entorhinal cortex atrophy in frontotemporal dementia and Alzheimer's disease. Neurology 52, 91–100.

Gao, F.Q., Black, S.E., Leibovitch, F.S., Callen, D.J., Lobaugh, N.J., Szalai, J.P., 2003. A reliable MR measurement of medial temporal lobe width from the Sunnybrook Dementia Study. Neurobiol. Aging 24, 49–56.

Gao, F.Q., Black, S.E., Leibovitch, F.S., Callen, D.J., Rockel, C.P., Szalai, J.P., 2004. Linear width of the medial temporal lobe can discriminate Alzheimer's disease from normal aging: the Sunnybrook Dementia Study. Neurobiol. Aging 25 (4), 441–448.

Goldszal, A.F., Davatzikos, C., Pham, D.L., Yan, M.X., Bryan, R.N., Resnick, S.M., 1998. An image-processing system for qualitative and quantitative volumetric analysis of brain images. J. Comput. Assist. Tomogr. 22, 827–837.

Good, C.D., Johnsrude, I.S., Ashburner, J., Henson, R.N., Friston, K.J., Frackowiak, R.S., 2001. A voxel-based morphometric study of ageing in 465 normal adult human brains. NeuroImage 14, 21–36.

Greenwood, P.M., 2000. The frontal aging hypothesis evaluated. J. Int. Neuropsychol. Soc. 6, 705–726.

Guttmann, C.R., Jolesz, F.A., Kikinis, R., Killiany, R.J., Moss, M.B., Sandor, T., Albert, M.S., 1998. White matter changes with normal aging. Neurology 50, 972–978.

Jack Jr., C.R., Petersen, R.C., O'Brien, P.C., Tangalos, E.G., 1992. MR-based hippocampal volumetry in the diagnosis of Alzheimer's disease. Neurology 42, 183–188.

Juottonen, K., Lehtovirta, M., Helisalmi, S., Riekkinen Sr., P.J., Soininen, H., 1998. Major decrease in the volume of the entorhinal cortex in patients with Alzheimer's disease carrying the apolipoprotein E epsilon4 allele. J. Neurol., Neurosurg. Psychiatry 65, 322–327.

Kesslak, J.P., Nalcioglu, O., Cotman, C.W., 1991. Quantification of magnetic resonance scans for hippocampal and parahippocampal atrophy in Alzheimer's disease. Neurology 41, 51–54.

Kim, J.J., Crespo-Facorro, B., Andreasen, N.C., O'Leary, D.S., Zhang, B., Harris, G., Magnotta, V.A., 2000. An MRI-based parcellation method for the temporal lobe. NeuroImage 11, 271–288.

Kohler, S., Black, S.E., Sinden, M., Szekely, C., Kidron, D., Parker, J.L., Foster, J.K., Moscovitch, M., Winocour, G., Szalai, J.P., et al., 1998. Memory impairments associated with hippocampal versus parahippocampal-gyrus atrophy: an MR volumetry study in Alzheimer's disease. Neuropsychologia 36, 901–914.

Kovacevic, N., Lobaugh, N.J., Bronskill, M.J., Levine, B., Feinstein, A., Black, S.E., 2002. A robust method for extraction and automatic segmentation of brain images. NeuroImage 17, 1087–1100.

Levine, B., Katz, D., Dade, L.A., Black, S., 2002. Novel approaches to the assessment of frontal damage and executive deficits in traumatic brain injury. In: Stuss, D.T., Knight, R. (Eds.), The Age of the Frontal Lobes. Oxford Univ. Press, New York, pp. 448–465.

Ono, M., Kubik, S., Abernathey, C.D., 1990. Atlas of the Cerebral Sulci Georg Thieme Verlag, New York.

Pfefferbaum, A., Mathalon, D.H., Sullivan, E.V., Rawles, J.M., Zipursky, R.B., Lim, K.O., 1994. A quantitative magnetic resonance imaging study of changes in brain morphology from infancy to late adulthood. Arch. Neurol. 51, 874–887.

Quarantelli, M., Larobina, M., Volpe, U., Amati, G., Tedeschi, E., Ciarmiello, A., Brunetti, A., Galderisi, S., Alfano, B., 2002. Stereotaxy-based regional brain volumetry applied to segmented MRI: validation and results in deficit and nondeficit schizophrenia. NeuroImage 17, 373–384.

Rademacher, J., Galaburda, A.M., Kennedy, D.N., Filipek, P.A., Caviness Jr., V.S., 1992. Human cerebral cortex: localization, parcellation, and morphometry with magnetic resonance imaging. J. Cogn. Neurosci. 4, 352–374.

Rademacher, J., Caviness Jr., V.S., Steinmetz, H., Galaburda, A.M., 1993. Topographical variation of the human primary cortices: implications for neuroimaging, brain mapping, and neurobiology. Cereb. Cortex 3, 313–329.

Raz, N., 2000. Aging of the brain and its impact on cognitive performance: integration of structural and functional findings. In: Craik, F.I.M., Salthouse, T.A. (Eds.), The Handbook of Aging and Cognition. Lawrence Erlbaum Associates, MahWah, NJ, pp. 1–90.

Raz, N., Gunning, F.M., Head, D., Dupuis, J.H., McQuain, J., Briggs, S.D., Loken, W.J., Thornton, A.E., Acker, J.D., 1997. Selective aging of the human cerebral cortex observed in vivo: differential vulnerability of the prefrontal gray matter. Cereb. Cortex 7, 268–282.

Resnick, S.M., Goldszal, A.F., Davatzikos, C., Golski, S., Kraut, M.A., Metter, E.J., Bryan, R.N., Zonderman, A.B., 2000. One-year age changes in MRI brain volumes in older adults. Cereb. Cortex 10, 464–472.

Resnick, S.M., Pham, D.L., Kraut, M.A., Zonderman, A.B., Davatzikos, C., 2003. Longitudinal magnetic resonance imaging studies of older adults: a shrinking brain. J. Neurosci. 23, 3295–3301.

Rosen, H.J., Gorno-Tempini, M.L., Goldman, W.P., Perry, R.J., Schuff, N., Weiner, M., Feiwell, R., Kramer, J.H., Miller, B.L., 2002. Patterns of brain atrophy in frontotemporal dementia and semantic dementia. Neurology 58, 198–208.

Salat, D.H., Kaye, J.A., Janowsky, J.S., 2001. Selective perseveration and degeneration within the prefrontal cortex in aging and Alzheimer disease. Arch. Neurol. 58, 1403–1408.

Salat, D.H., Kaye, J.A., Janowsky, J.S., 2002. Greater orbital prefrontal volume selectively predicts worse working memory performance in older adults. Cereb. Cortex 12, 494–505.

Shrout, P., Fleiss, J., 1979. Intraclass correlations: uses in assessing rater reliability. Psycholog. Bull., 420–428.

Steinmetz, H., Fürst, G., Freund, H.J., 1989. Cerebral cortical localization: application and validation of the proportional grid System in MR imaging. J. Comput. Assist. Tomogr. 13, 10–19.

Talairach, J., Tournoux, P., 1988. Co-Planar Stereotaxic Atlas of the Human Brain. Thieme Medical, New York.

Tisserand, D.J., Visser, P.J., van Boxtel, M.P., Jolles, J., 2000. The relation between global and limbic brain volumes on MRI and cognitive performance in healthy individuals across the age range. Neurobiol. Aging 21, 569–576.

Tisserand, D.J., Pruessner, J.C., Sanz Arigita, E.J., van Boxtel, M.P., Evans, A.C., Jolles, J., Uylings, H.B., 2002. Regional frontal cortical volumes decrease differentially in aging: an MRI study to compare volmetric approaches and voxel-based morphometry. NeuroImage 17, 657–669.

Tzourio-Mazoyer, N., Landeau, B., Papathanassiou, D., Crivello, F., Etard, O., Delcroix, N., Mazoyer, B., Joliot, M., 2002. Automated anatomical labeling of activations in SPM using a macroscopic anatomical parcellation of the MNI MRI single-subject brain. NeuroImage 15, 273–289.

Watkins, K.E., Paus, T., Lerch, J.P., Zijdenbos, A., Collins, D.L., Neelin, P., Taylor, J., Worsley, K.J., Evans, A.C., 2001. Structural asymmetries in the human brain: a voxel-based statistical analysis of 142 MRI scans. Cereb. Cortex 11, 868–877.

Woods, R.P., Grafton, S.T., Holmes, C.J., Cherry, S.R., Mazziotta, J.C., 1998. Automated image registration: I. General methods and intrasubject, intramodality validation. J. Comput. Assist. Tomogr. 22, 139–152.